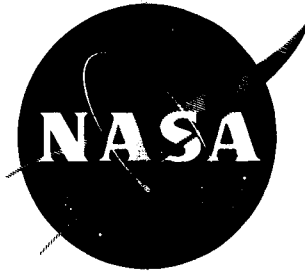


27p.



N68 19277

Code-1

TECHNICAL NOTE

D-1940

AN INVESTIGATION OF THE
NATURAL FREQUENCIES AND MODE SHAPES OF
DOUBLE CONICAL SANDWICH DISKS

By William M. Thompson, Jr., and Robert R. Clary

Langley Research Center
Langley Station, Hampton, Va.

NATIONAL AERONAUTICS AND SPACE ADMINISTRATION
WASHINGTON

August 1963

NATIONAL AERONAUTICS AND SPACE ADMINISTRATION

TECHNICAL NOTE D-1940

AN INVESTIGATION OF THE
NATURAL FREQUENCIES AND MODE SHAPES OF
DOUBLE CONICAL SANDWICH DISKS

By William M. Thompson, Jr., and Robert R. Clary

SUMMARY

An experimental investigation was conducted to determine, by induced oscillation, the resonant frequencies and nodal patterns of some shallow sandwich disks having a radially symmetric thickness linearly tapered from a maximum thickness at the center. Two types of supports were employed: one in which the disk center was pinned and a second in which the disks were hung on soft supports which offered negligible restraint against motion. Measured results are presented and differences in the response of aluminum-honeycomb- and styrofoam-core models are indicated and discussed. The lower normal mode resonant frequencies were calculated by the application of an existing analytical method. A comparison of calculated and measured frequencies showed fair agreement for models with a honeycomb core but, in general, showed poor agreement for the modes of models with a styrofoam core.

INTRODUCTION

The current philosophy in space-vehicle structural design indicates an increasing trend toward the use of sandwich construction as a primary structural component. The basic advantage of this type of structure lies in its high flexural rigidity and buckling strength for relatively low weight. These ideal strength and weight features have prompted several theoretical investigations of uniform sandwich beams and flat plates under static and dynamic loading. (See, for example, ref. 1.) In addition, experimental data consisting of measurements of mechanical and other physical properties of a variety of core materials have been published. (See, for example, ref. 2.) There is, however, a marked absence in available literature of experimental data in the field of sandwich structural vibrations.

The present report seeks to contribute data in this area by presenting the results of vibration tests on a series of shallow sandwich disks of radially symmetric thickness and tapered linearly from the center as illustrated in figure 1.

The disks were 1/4-scale models of a proposed driving element (or loudspeaker) for a facility to generate low-frequency noise at the Langley Research Center. The driving element was 14 feet in diameter and was required to be a structure of high stiffness-to-weight ratio with natural frequencies above the range of noise frequencies to be generated by the facility (0 to 50 cps). The models were built and tested to provide vibration and fatigue data to aid in the detailed design of the full-scale driving element.

The data are presented in terms of resonant frequencies and nodal patterns of models with unrestrained edges and the center either fixed or suspended on soft supports which offered little or no resistance against motion. For all practical purposes, however, the disk in the latter case is considered unrestrained. Some of the frequencies are compared with calculated frequencies obtained by application of the theory in reference 3.

SYMBOLS

| | |
|-------|---|
| D | face plate flexural rigidity at radial coordinate r , $\frac{EI}{1 - \mu^2}$ |
| E | Young's modulus of faces |
| f | frequency |
| g | acceleration due to gravity |
| I | area moment of inertia per unit width of face plates about neutral surface at radial coordinate r , neglecting moments of inertia of the facings about their centroid, $\frac{t_f(t_{c,max})^2}{2} \left[\left(\frac{R - r}{R} \right)^2 + \frac{2t_f}{t_{c,max}} \left(\frac{R - r}{R} \right) + \left(\frac{t_f}{t_{c,max}} \right)^2 \right]$ |
| n | number of nodal diameters |
| R | radius of model |
| r | radial coordinate |
| T | kinetic energy |
| t_c | core thickness at radial coordinate r , $\frac{t_{c,max}}{R}(R - r)$ |
| t_f | face plate thickness |
| t_m | model thickness at hub, $t_{c,max} + 2t_f$ |
| V | potential energy in bending |

W_c weight per unit area of core material, $t_c \rho_c$
 W_f weight per unit area of face plate and bonding material
 w deflection of model
 w_0 mode shape
 θ angular coordinate
 μ Poisson's ratio
 ρ_c weight density of core material
 τ time
 ω angular frequency, $2\pi f$

Subscript:

max maximum

Dots over symbols denote differentiation with respect to time.

EXPERIMENTAL INVESTIGATION

Apparatus

Model description.- Four 42-inch-diameter models were fabricated for vibration testing. Two models, designated H, contained an aluminum honeycomb core and the other two, designated F, contained a closed cell styrofoam core material. The honeycomb core used in the H models had a cell size of $3/8$ inch and a wall thickness of 0.002 inch. As shown in figure 2, each model consisted of a circular, radially symmetric, core slab linearly tapered from the center and covered by a thin aluminum skin facing 0.016 inch thick. In order to avoid complicated pre-shaping of the face plates to fit the core taper, each facing was constructed from two sections bonded at butt-lap seams (fig. 2, section C-C) running diametrically along the model surface. In a completed structure, the seam in one facing was oriented 90° to the seam in the opposite face.

Pertinent structural parameters and elastic constants of the four models are given in table I. The values given in table I for the shear modulus and density of the core materials were obtained from literature supplied by the manufacturer. The aluminum honeycomb is orthotropic in shear having a shear modulus of 39,000 psi in one direction (designated the ribbon axis) and 19,000 psi in the normal or transverse direction. The core material was bonded to the skin and center hub by using a mixture of $2\frac{1}{2}$ parts of Products Research Co. PR-1421 polysulfide elastomer to 100 parts of Armstrong Products Co. A-6 adhesive. The

honeycomb cores were machined from continuous sections of material whereas the foam cores were cut from styrofoam slabs consisting of four sections (each 1 foot in width) attached by bonded butt joints. Photographs taken prior to final assembly of the models are shown in figure 3. The line visible on the honeycomb core is a slight indentation caused by the butt-lap seam in the face plate.

Instrumentation.- The mechanism for inducing oscillation and the instrumentation utilized in the vibration tests are shown schematically in figure 4. Model excitation was induced by an electromagnetic shaker.

Response of the model to induced vibration was measured by a crystal accelerometer having a sensitivity of 4.65 mv/g root mean square. The output voltage from this transducer was amplified by a cathode follower which provided a sensing system with a flat response (± 5 percent) for frequencies ranging from 20 to 6,000 cps. The amplified signal from the accelerometer together with the shaker oscillator signal was monitored with a cathode ray oscilloscope from which resonant frequencies and phase shifts in the motion of the model were detected by observing disk response amplitude and Lissajous figures, respectively. In the cases where mode shapes were obtained, the root-mean-square output voltage of the transducer was measured by a Ballantine voltmeter.

Test Procedure

Translational oscillation of the four models was induced to obtain resonant frequencies and associated nodal patterns. Two sets of boundary conditions were imposed: fixed center and unrestrained. The fixed-center condition was achieved by attaching the model to a 3/4-inch steel shaft of sufficient length to pass through the hole in the model hub. The extremities of the shaft were secured to massive structures in order to minimize any rigid-body motion of the model relative to its plane of symmetry. The unrestrained condition was accomplished by securing in the hub hole a lightweight rod to which strings were attached to support the model. For the fixed-center boundary condition the shaker was attached at the rim of the model, whereas for the unrestrained boundary condition the shaker was attached to the hub rod. Details of the support systems are shown in figure 5. Because of the weight of the movable coil in the shaker, an effective mass was added to the model at the point of shaker attachment. The weight of the core in the shaker used was 0.6 pound, and no effort was made to correct for the presence of this mass in the experimental or analytical results. The total weights of the models varied from about 8 to 11 pounds. (See table I.)

For some models, mode shapes were obtained. These data consisted of measuring the relative amplitude of the acceleration at points along a radial line on the face-plate surface. These cases were restricted to resonant frequencies having nodal patterns comparable to patterns exhibited in the vibration of thin, homogeneous plates of uniform thickness. Unfortunately, mode shapes were not obtained for the H-6 model since it underwent structural alteration after the initial vibration tests. (The number following the letter in the model designations denotes the nominal hub thickness.)

In tests involving all models for the fixed-center boundary condition, the electromagnetic shaker was attached to the model rim at the same position relative to the facing seam. The influence on natural frequency and nodal patterns due to change of the position of the shaker attachment was investigated. No appreciable effect on the resonant frequencies was evident; however, nodal diameters shifted position so as to appear always in the same locations on the facing relative to the shaker attachment point.

DATA PRESENTATION AND DISCUSSION

General Remarks

Compared to a uniform, homogeneous plate of a constant weight per unit area, the elastic behavior of a comparable sandwich structure is relatively complex. Because of the low rigidity of the core material, sandwich-plate theory indicates that some deflection may be attributed to shear effects. In addition, either or both of the facings and core may have orthotropic elastic characteristics which impose the same properties on the model as a unit. The models used in the tests discussed herein represent structures having isotropic facings and, in the case of the honeycomb-core models, orthotropic cores.

The test results consist of nodal patterns at resonances for each model in a frequency spectrum ranging up to approximately 650 cps (figs. 6 to 9). Some measured mode shapes are also presented which enable comparison of the deflection patterns of models having styrofoam cores and aluminum honeycomb cores (figs. 10 to 12). In general, the models with the honeycomb core had higher frequencies than the models with the styrofoam core; this may be due in part to the large differences in stiffness between honeycomb and styrofoam, as indicated by the shear moduli shown in table I.

Honeycomb core.— The node patterns obtained at resonant frequencies during excitation of the honeycomb-core models are shown in figures 6 and 7 for the fixed-center boundary condition and the unrestrained boundary condition, respectively, and, in general, show more or less classical patterns. For the fixed-center boundary condition in particular, both models exhibit, for the most part, nodal patterns representative of the normal modes of a homogeneous plate of uniform thickness.

A significant feature displayed by the data is the existence, in some cases, of two resonant frequencies with essentially the same nodal pattern, except for shifts in nodal position from one frequency to the other. Examples may be seen in figure 6 for the four-node and six-node frequencies of model H-3 and also for the single-node frequencies of model H-6 in figure 7. This effect has been noted in reference 4 during excitation of the breathing modes of a cylindrical shell and is explained on the basis of the more general investigation of reference 5. The occurrence of double resonance peaks in elastic bodies of revolution is quite common due to: (a) structural deviation from rotational symmetry inherent in fabrication, and (b) imperfections in material. The existence of these deviations in a structure produces two preferential planes of vibration and thus two resonant

frequencies for each mode. Therefore, excitation in any other plane can produce a double resonance. Since the models used in these tests were not manufactured within precision tolerances, there is a high probability that structural asymmetry permits the occurrence of the double resonance peaks observed. Moreover, in light of reference 5, the wide spread in frequency between the two resonant peaks, particularly for model H-6, indicates that the imperfections may be quite large.

Styrofoam core.- The nodal patterns obtained at resonant frequencies during excitation of the styrofoam-core models are shown in figures 8 and 9 for the fixed-center boundary condition and the unrestrained boundary condition, respectively. In the data shown in these figures, there is a marked predominance of erratic nodal patterns associated with the higher modes. In an effort to learn whether or not this behavior could be linked to failure in the styrofoam core or in the face-to-core bonding, model F-3 was completely disassembled. The core appeared to be undamaged and the face-to-core bond intact except for the relatively small areas shown in figure 13 where bonding had evidently not been achieved during construction of the model. Thus, the explanation for the erratic nodal patterns remains unknown.

It is interesting to note that figures 8 and 9 also indicate the tendency for two resonant frequencies to exhibit the same nodal patterns. (For example, compare the sixth and seventh frequencies ($f = 465$ and 485 cps) of model F-3 in figure 8(a) with the third and fourth frequencies ($f = 509$ and 555 cps) of model F-6 in figure 9(b).) This effect has been discussed in connection with the honeycomb-core models where more examples of the phenomenon were observed.

Mode Shapes

Honeycomb core.- Deflections of the honeycomb-core model (H-3) were measured at some of the lower modes and results are shown in figure 10. Deflection curves were normalized to the maximum value at each frequency, and peak accelerations and deflections corresponding to unity in the mode shapes are given in table II. The mode shapes in figure 11 indicate a predominance of bending similar to that obtained from bending of a uniform, homogeneous plate. As previously indicated, no deflection patterns were obtained for the H-6 model.

Styrofoam core.- Normalized mode shapes are presented in figures 11 and 12 for the F-3 and F-6 models, respectively, and the peak accelerations and deflections corresponding to unity in the graphs are also presented in table II. A comparison of the mode shapes of comparable F-3 and F-6 nodal patterns shows that a qualitative similarity exists between the deflection of the two models. The curvature of the mode shapes of the styrofoam-core model, in contrast with the curvature of the mode shapes of the honeycomb-core model, is significantly different from that expected on the basis of bending theory, especially for the fixed-center "dishing" mode and the unrestrained mode with one nodal circle. Unfortunately, no explanation can be given for the occurrence of these peculiar deflection curves.

ANALYSIS

Calculation of Frequency Equations

The computation of natural frequencies for the lower modes is based on the Rayleigh energy method. The expressions for strain energy and kinetic energy are those given in reference 3 for the classical bending of plates in which shear effects are neglected. In the application of the theory, the structure is assumed to be isotropic and the disk stiffness is assumed to be variable.

The total strain energy V in a circular isotropic plate or disk due to bending is given in polar coordinates r, θ in reference 3 as

$$V = \int_0^R \int_0^{2\pi} \frac{D}{2} \left\{ \left[\frac{\partial^2 w}{\partial r^2} + \frac{1}{r} \frac{\partial w}{\partial r} + \frac{1}{r^2} \frac{\partial^2 w}{\partial \theta^2} \right]^2 - 2(1 - \mu) \frac{\partial^2 w}{\partial r^2} \left(\frac{1}{r} \frac{\partial w}{\partial r} + \frac{1}{r^2} \frac{\partial^2 w}{\partial \theta^2} \right) + 2(1 - \mu) \left[\frac{\partial}{\partial r} \left(\frac{1}{r} \frac{\partial w}{\partial \theta} \right) \right]^2 \right\} r \, dr \, d\theta \quad (1)$$

and the kinetic energy T of the vibrating disk is

$$T = \frac{1}{2g} \int_0^R \int_0^{2\pi} (W_f + W_c) \dot{w}^2 r \, dr \, d\theta \quad (2)$$

In these expressions, the stiffness D is given by

$$D \approx \frac{Et_f(t_{c,\max})^2}{2(1 - \mu^2)} \left[\left(\frac{R - r}{R} \right)^2 + \frac{2t_f}{t_{c,\max}} \left(\frac{R - r}{R} \right) + \left(\frac{t_f}{t_{c,\max}} \right)^2 \right]$$

where

W_f weight per unit area of face plates and bonding material

W_c weight per unit area of core material, $t_c \rho_c$

μ Poisson's ratio

Since $\left(\frac{t_f}{t_{c,\max}} \right) \ll 1$, $\left(\frac{t_f}{t_{c,\max}} \right)^2$ is neglected in the calculation of D . The procedure consists of assuming a deflection of the form $w = w_0(r, \theta) \cos \omega t$ and substituting w in equations (1) and (2) to give the following expressions for the maximum potential and kinetic energies:

$$V_{\max} = \int_0^R \int_0^{2\pi} \frac{D}{2} \left\{ \left[\frac{\partial^2 w_0}{\partial r^2} + \frac{1}{r} \frac{\partial w_0}{\partial r} + \frac{1}{r^2} \frac{\partial^2 w_0}{\partial \theta^2} \right]^2 - 2(1 - \mu) \frac{\partial^2 w_0}{\partial r^2} \left(\frac{1}{r} \frac{\partial w_0}{\partial r} + \frac{1}{r^2} \frac{\partial^2 w_0}{\partial \theta^2} \right) \right. \\ \left. + 2(1 - \mu) \left[\frac{\partial}{\partial r} \left(\frac{1}{r} \frac{\partial w_0}{\partial \theta} \right) \right]^2 \right\} r \, dr \, d\theta \quad (3)$$

and

$$T_{\max} = \frac{\omega^2}{2g} \int_0^R \int_0^{2\pi} (W_f + W_c) w_0^2 r \, dr \, d\theta \quad (4)$$

The function w_0 constitutes the mode shape and is assumed such that the geometric boundary conditions of the disk (deflection and slope at the center and the edge) are satisfied. Once an appropriate w_0 is chosen, the natural frequency for a particular mode shape can be calculated from the relation $V_{\max} - T_{\max} = 0$.

In this investigation, the mode shape

$$w_0 = \left(\frac{r}{R} \right)^2 \cos n\theta$$

was chosen for the fixed-center condition (n nodal diameters) and the mode shape

$$w_0 = 1 - 2 \left(\frac{r}{R} \right)^2$$

was chosen for the unrestrained condition (one nodal circle). With $W_f = 0.00424$ lb/sq in. and $\mu = 1/3$, the frequency equations corresponding to these two boundary conditions are, respectively,

$$f_n = \frac{1}{2\pi R^2} \sqrt{\frac{\frac{21}{32} E g t_f (3n^4 - 12n^2 + 32) [(t_{c,\max})^2 + 4t_{c,\max} t_f]}{7W_f + t_{c,\max} \rho_c}} \quad (5)$$

and

$$f = \frac{1}{2\pi R^2} \sqrt{\frac{420 E g t_f [(t_{c,\max})^2 + 4t_{c,\max} t_f]}{35W_f + 13\rho_c t_{c,\max}}} \quad (6)$$

Calculated Results and Comparisons With Experiment

The natural frequencies for models H-3 and H-6 calculated from equations (5) and (6) are plotted in figure 14(a) for the indicated modes as a function of the ratio of maximum core thickness $t_{c,max}$ to radius R . The experimental results are included for comparison. Fair agreement exists between the calculated and measured natural frequencies of the honeycomb-core models for the range of frequencies covered in the present tests.

The calculated frequencies of the styrofoam-core models are shown in figure 14(b), where rather poor agreement is evident between experimental and calculated frequencies for the fixed-center dishing mode and the unrestrained single nodal circle mode. Since the measured mode shapes (figs. 11 and 12) show a deflection pattern opposite in curvature to the shape assumed w_0 for overall bending of the model in the frequency calculation, the disagreement in these results is not unreasonable. In the case of the fixed-center mode with 2 nodal diameters, the assumed mode shape w_0 agrees more favorably with measured deflection as shown in figures 11 and 12, and the frequencies obtained for this particular case show satisfactory agreement.

It should be emphasized that the fair agreement noted in the calculated and experimental natural frequencies of some models does not imply that the dynamic behavior of sandwich structures may generally be predicted on the basis of simple theory. At best, the calculation presented herein can be considered only a gross approximation.

CONCLUDING REMARKS

Radially symmetric sandwich disks linearly tapered from a maximum thickness at the center and having aluminum face plates were subjected to forced vibration in a frequency spectrum ranging up to approximately 650 cps. Two different core materials were utilized in the models: aluminum honeycomb and closed cell styrofoam. Measured natural frequencies, nodal patterns, and mode shapes of the sandwich models were obtained with the center fixed and with the model freely suspended with negligible restraint against motion. In addition, some low mode frequencies calculated by means of the Rayleigh energy method are presented and compared with experimentally determined values. The results of this investigation lead to the following general observation:

The resonant frequencies of the models with the honeycomb core in the test range exhibited nodal patterns which, in general, correspond to the normal flexural modes of a homogeneous plate of uniform thickness. Mode shapes measured at different points on radial lines of the disk also indicate deflection shapes resembling those observed in the bending of homogeneous plates. Theoretical and measured resonant frequencies for low normal modes show fair agreement.

Similar data obtained with the models having a styrofoam core show, in general, a somewhat different response. Erratic nodal patterns were observed for frequencies usually above the second mode for the fixed-center and unrestrained

boundary conditions. Comparison of calculated and measured natural frequencies of the fixed-center dishing mode and the mode of the freely suspended model with one nodal circle disagree by nearly 3 to 1, whereas these results for the fixed-center mode with 2 nodal diameters show favorable agreement.

An overall comparison of the natural frequencies between models with honeycomb cores and styrofoam cores for comparable nodal patterns indicates that, generally, frequencies were lower for the models with the styrofoam core.

Langley Research Center,
National Aeronautics and Space Administration,
Langley Station, Hampton, Va., May 10, 1963.

REFERENCES

1. Yu, Yi-Yuan: Simplified Vibration Analysis of Elastic Sandwich Plates. Jour. Aerospace Sci., vol. 27, no. 12, Dec. 1960, pp. 894-900.
2. Voss, A. W.: Mechanical Properties of Some Low-Density Materials and Sandwich Cores. Rep. No. 1826, Forest Products Lab., U.S. Dept. Agriculture, Mar. 1952.
3. Timoshenko. S.: Vibration Problems in Engineering. Second Ed., D. Van Nostrand Co., Inc., 1937, p. 426.
4. Lindholm, Ulric S., Kana, Daniel D., and Abramson, H. Norman: Breathing Vibrations of a Circular Cylindrical Shell With an Internal Liquid. Jour. Aerospace Sci., vol. 29, no. 9, Sept. 1962, pp. 1052-1059.
5. Tobias, S. A.: A Theory of Imperfection for the Vibrations of Elastic Bodies of Revolution. Engineering, vol. 172, no. 4470, Sept. 28, 1951, pp. 409-410.

TABLE I
STRUCTURAL CHARACTERISTICS OF MODELS

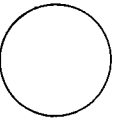
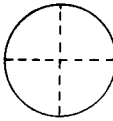
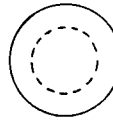
[$E = 10^7$ psi; $t_F = 0.016$ inch]

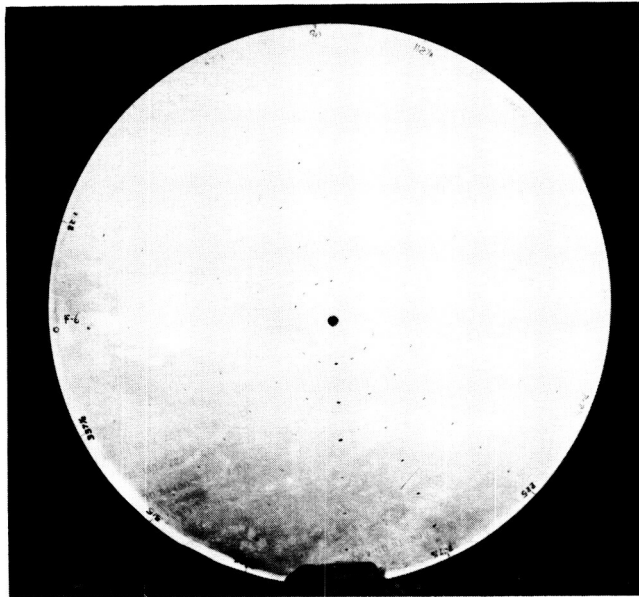
| Model (a) | Total weight, lb | t_m , in. | Core material | ρ_c , lb/cu ft | Core shear modulus, psi (b) |
|--------------|------------------------|----------------|-----------------------|------------------------|--------------------------------------|
| H-3 | 9.2 | 3.385 | Aluminum honeycomb | 3.15 | 19,000 |
| H-6 | 11.2 | 5.826 | | | 39,000 |
| F-3 | 8.1 | 3.385 | Styrofoam | 2.0 | 1,200 |
| F-6 | 9.4 | 5.826 | | | |

^aThe number following the core designation (letter) of each model denotes the nominal hub thickness.

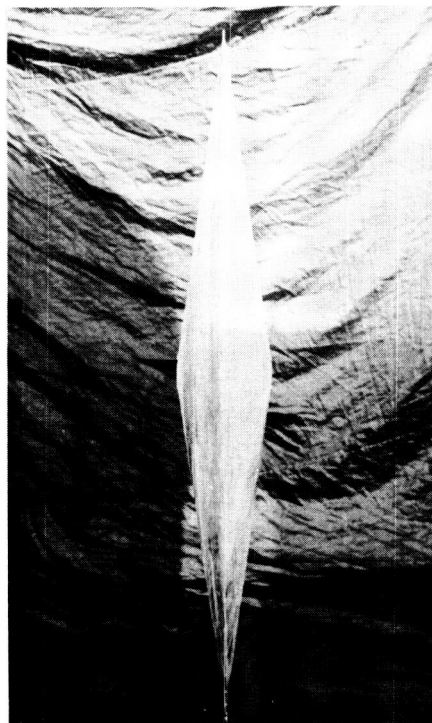
^bSmaller value of shear modulus for honeycomb models applies in transverse direction and larger value in the ribbon direction.

TABLE II
MODEL MAXIMUM RESPONSE

| Boundary condition | Mode | H-3 model | | | F-3 model | | | F-6 model | | |
|--------------------|---|-----------------------|----------------------|----------------|-----------------------|----------------------|----------------|-----------------------|----------------------|----------------|
| | | Acceleration, g units | Deflection, in. | Frequency, cps | Acceleration, g units | Deflection, in. | Frequency, cps | Acceleration, g units | Deflection, in. | Frequency, cps |
| Fixed center |  | 1.4 | 0.3×10^{-3} | 189 | 1.4 | 1.4×10^{-3} | 100 | 1.6 | 0.9×10^{-3} | 130 |
| |  | 2.6 | 0.4×10^{-3} | 248 | 4.6 | 0.8×10^{-3} | 233 | 2.5 | 0.2×10^{-3} | 344 |
| Unrestrained |  | 3.7 | 0.3×10^{-3} | 360 | 2.8 | 0.3×10^{-3} | 275 | 1.9 | 0.1×10^{-3} | 380 |



Plan view



Edge view

L-63-3153

Figure 1.- Model configuration.

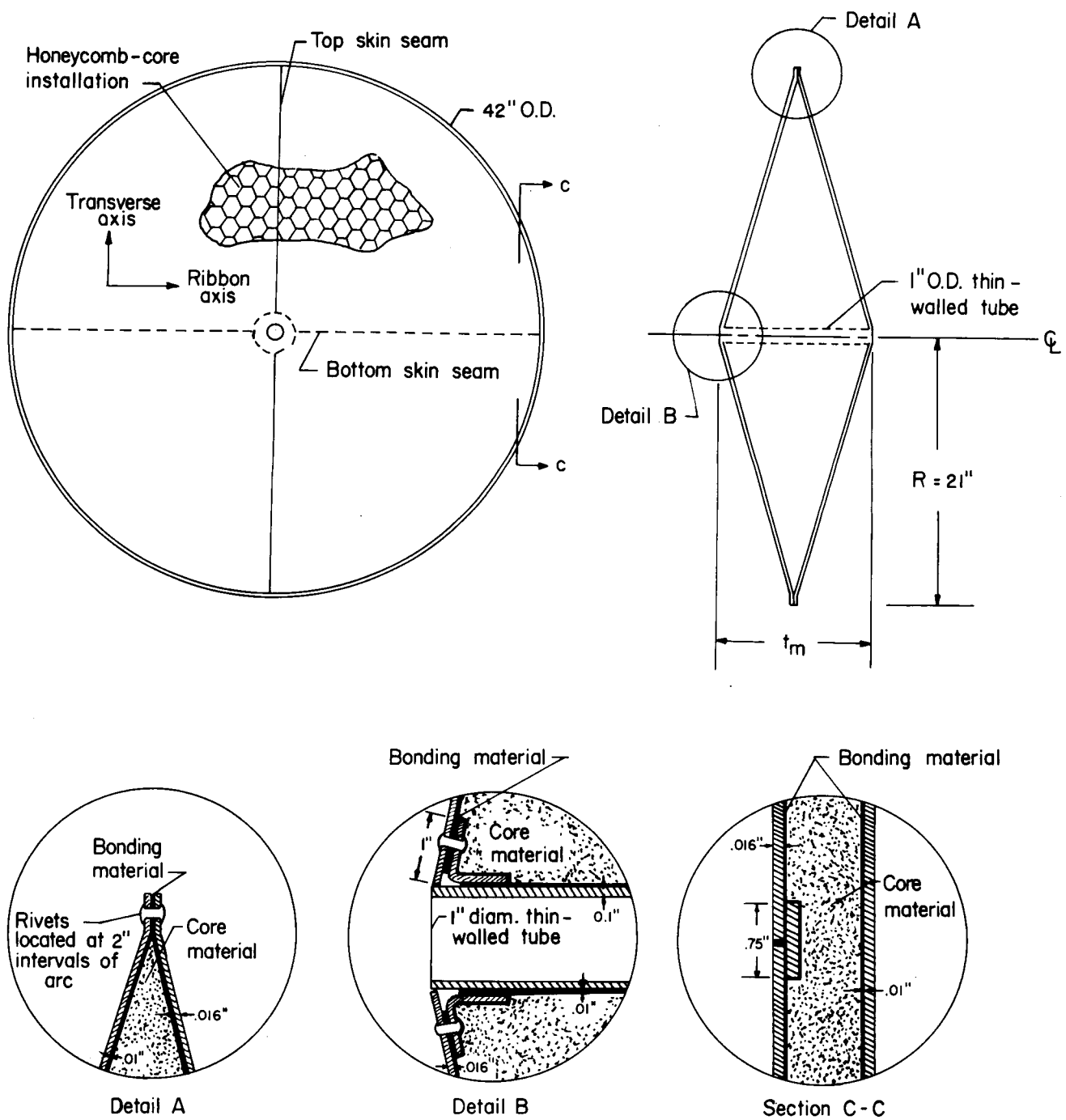
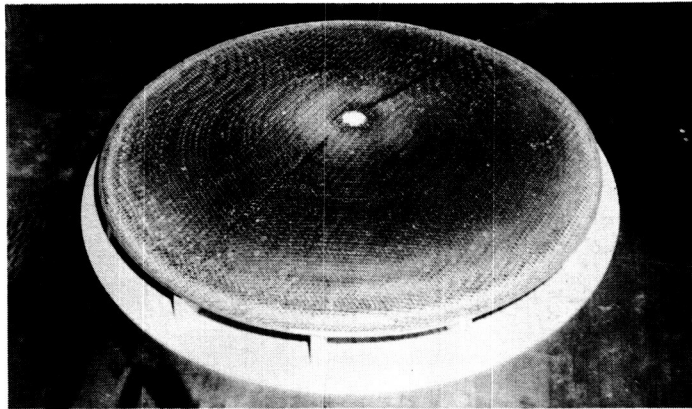
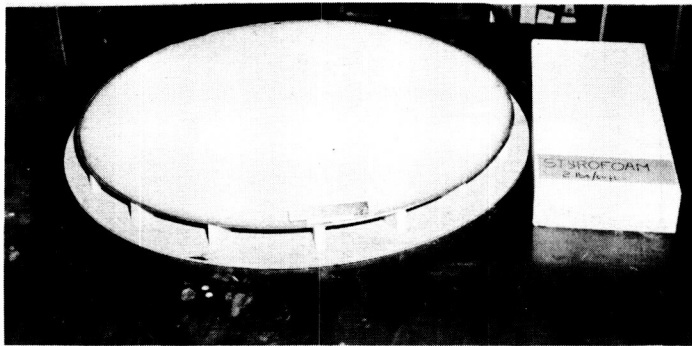


Figure 2.- Basic cone design (not to scale).



Honeycomb core



Styrofoam core



Face plate

L-63-3154

Figure 3.- Partially assembled honeycomb- and styrofoam-core models.

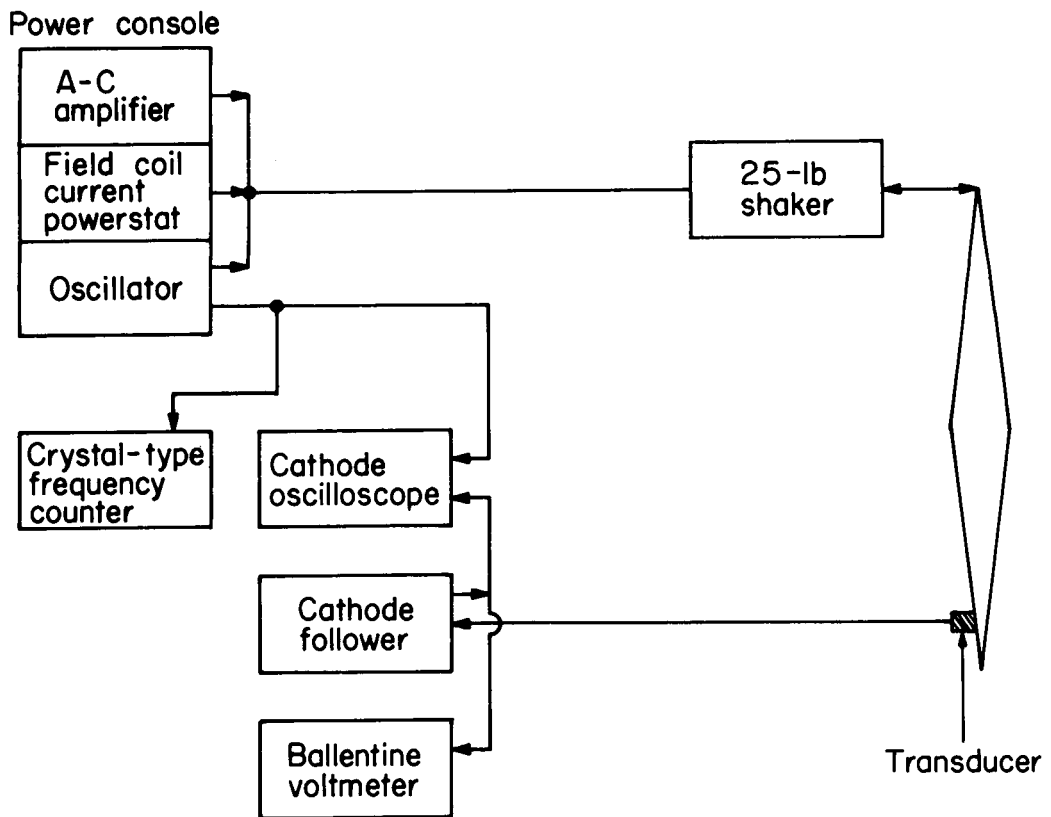
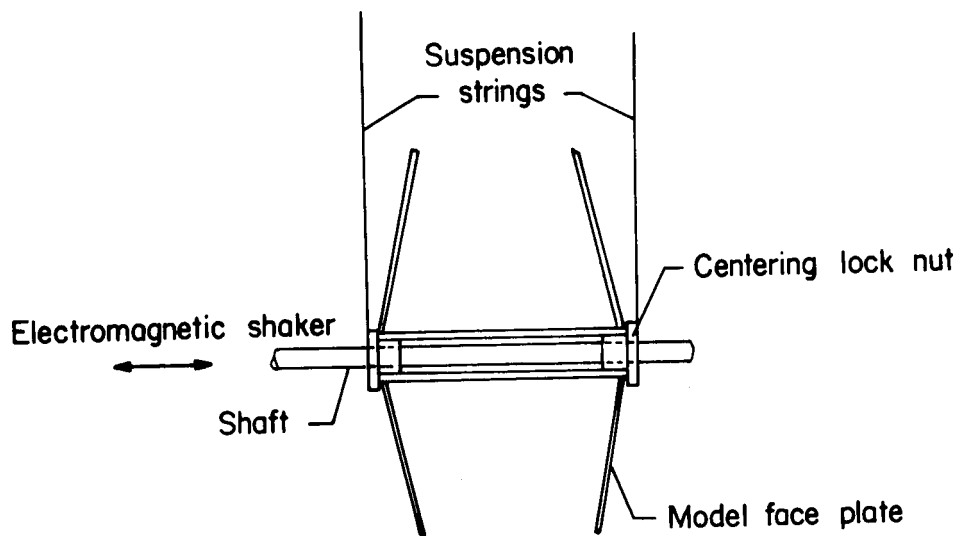
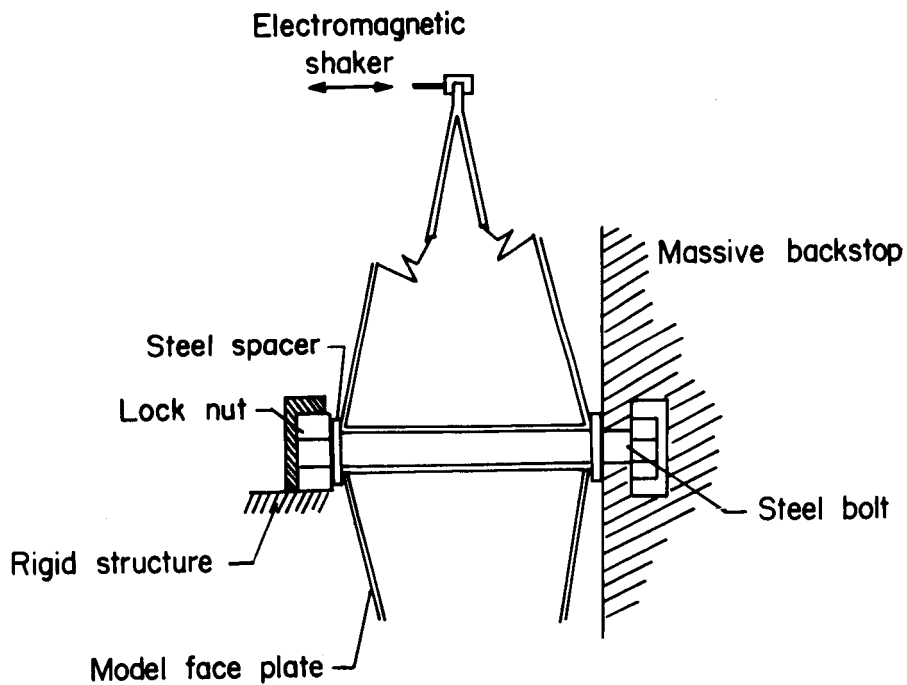


Figure 4.- Instrumentation block diagram for fixed-center configuration.



Unrestrained suspension



Fixed center

Figure 5.- Unrestrained and fixed-center boundary details (not to scale).

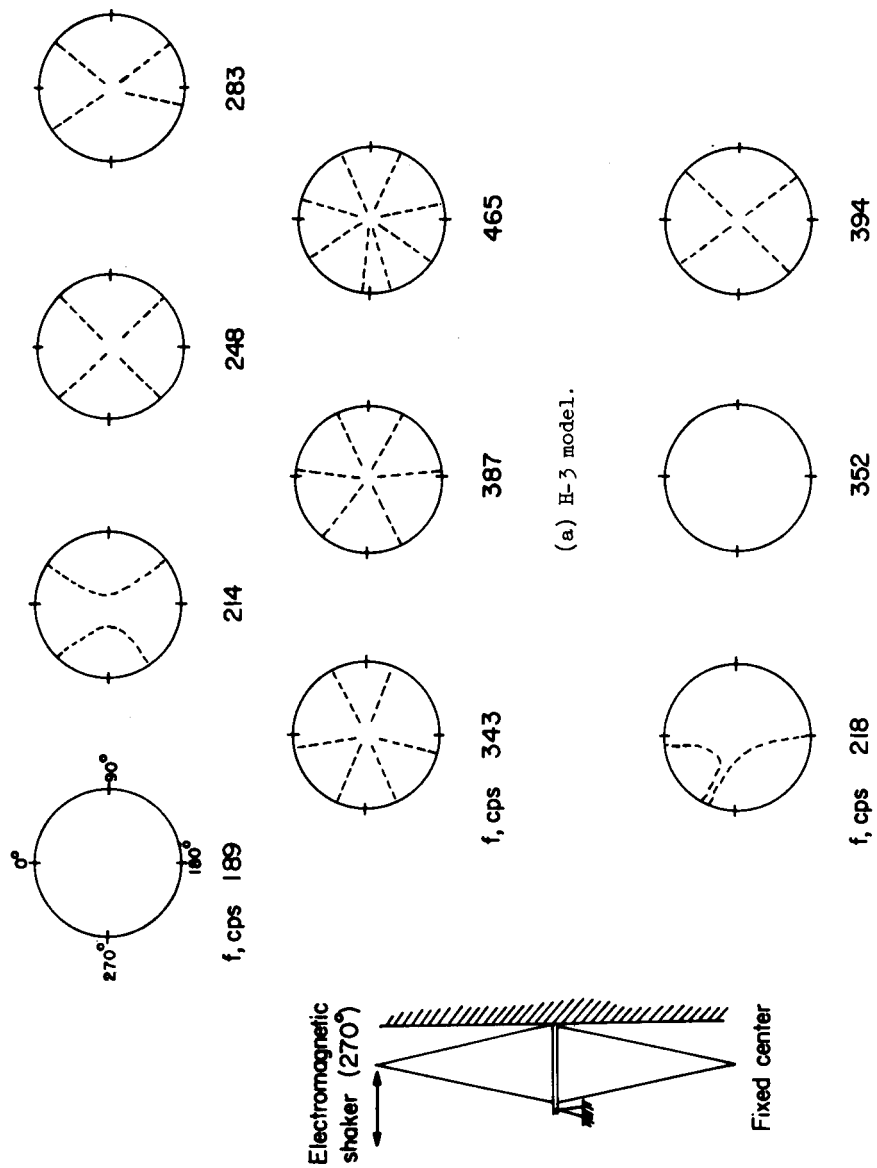


Figure 6.- Honeycomb-core node patterns for fixed-center boundary condition.

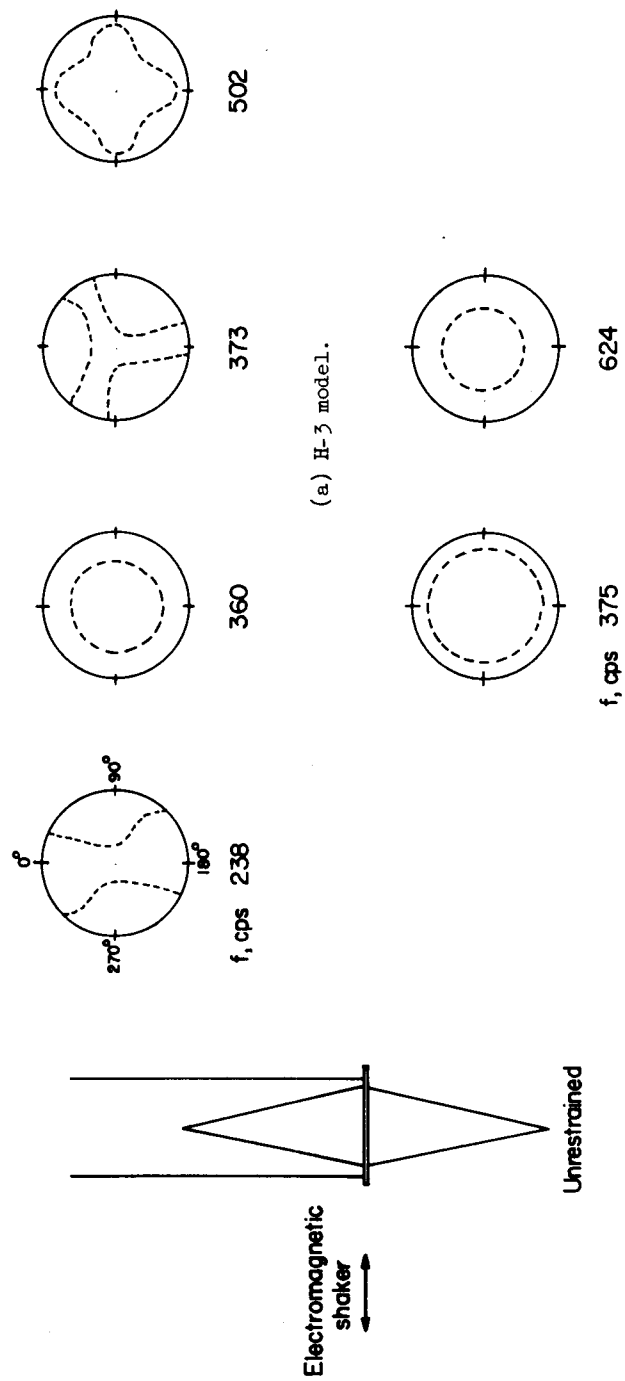


Figure 7.- Honeycomb-core node patterns for unrestrained boundary condition.

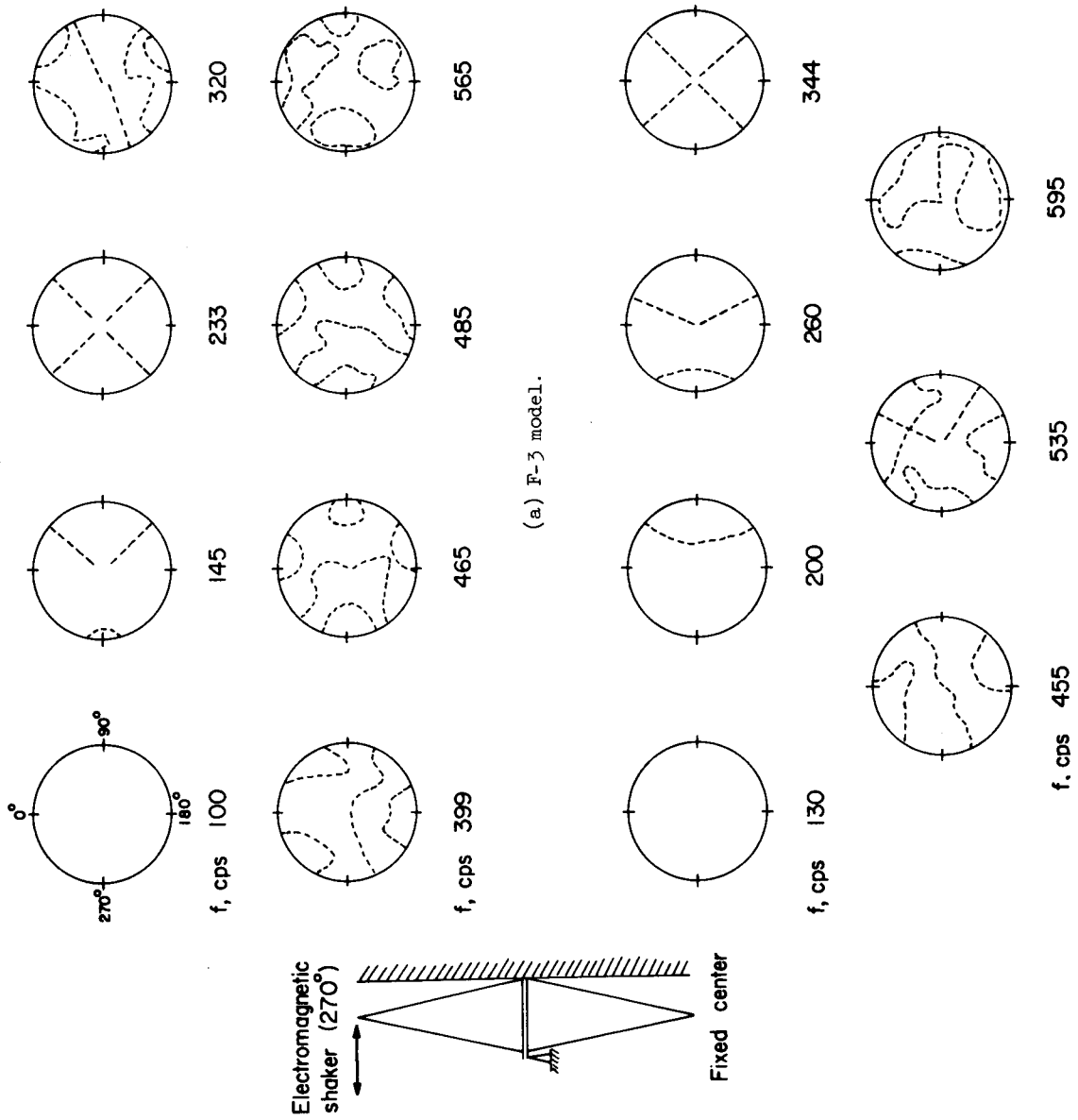


Figure 8.- Styrofoam-core node patterns for fixed-center boundary condition.

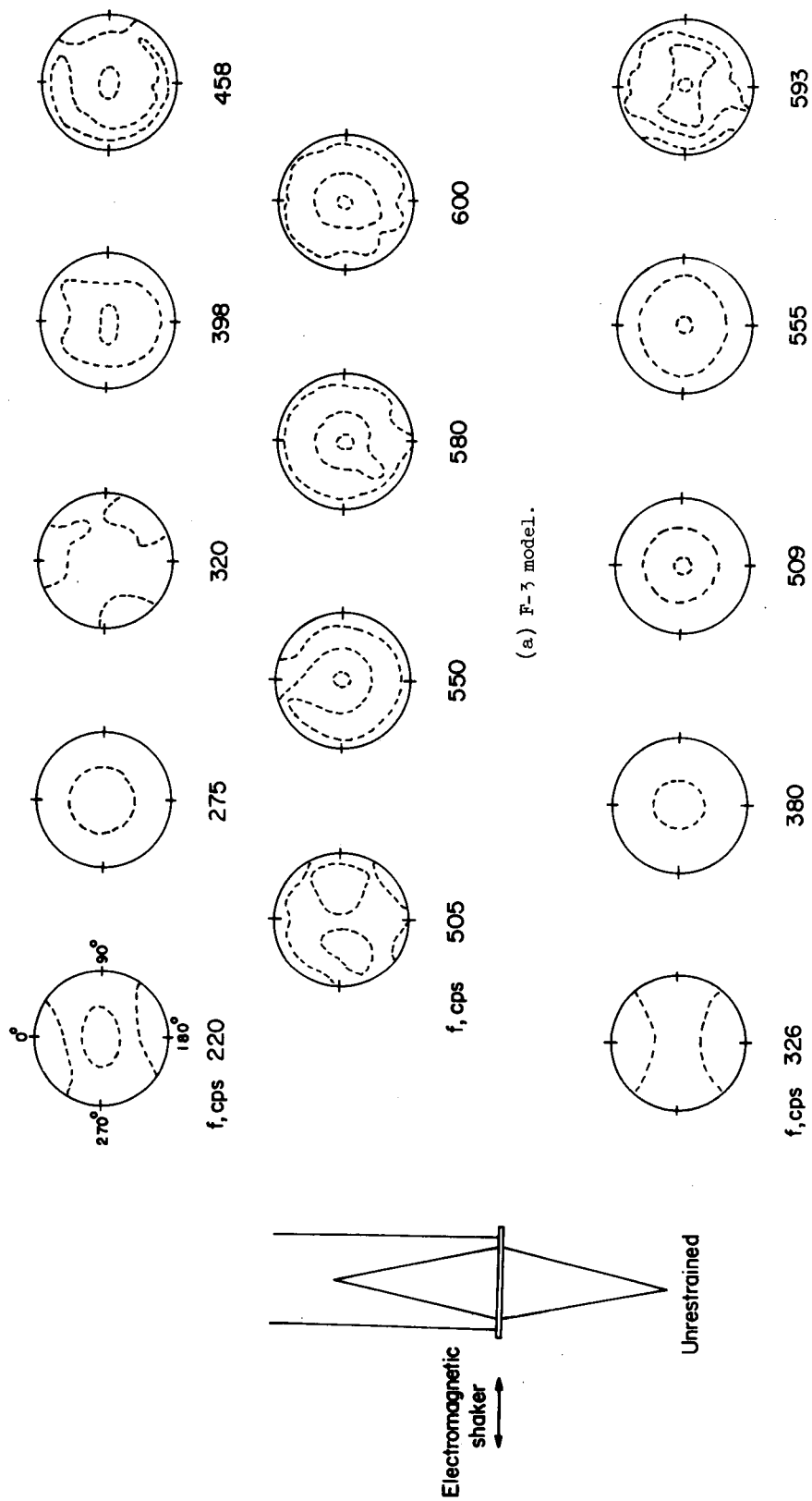


Figure 9.- Styrofoam-core node patterns for unrestrained boundary condition.

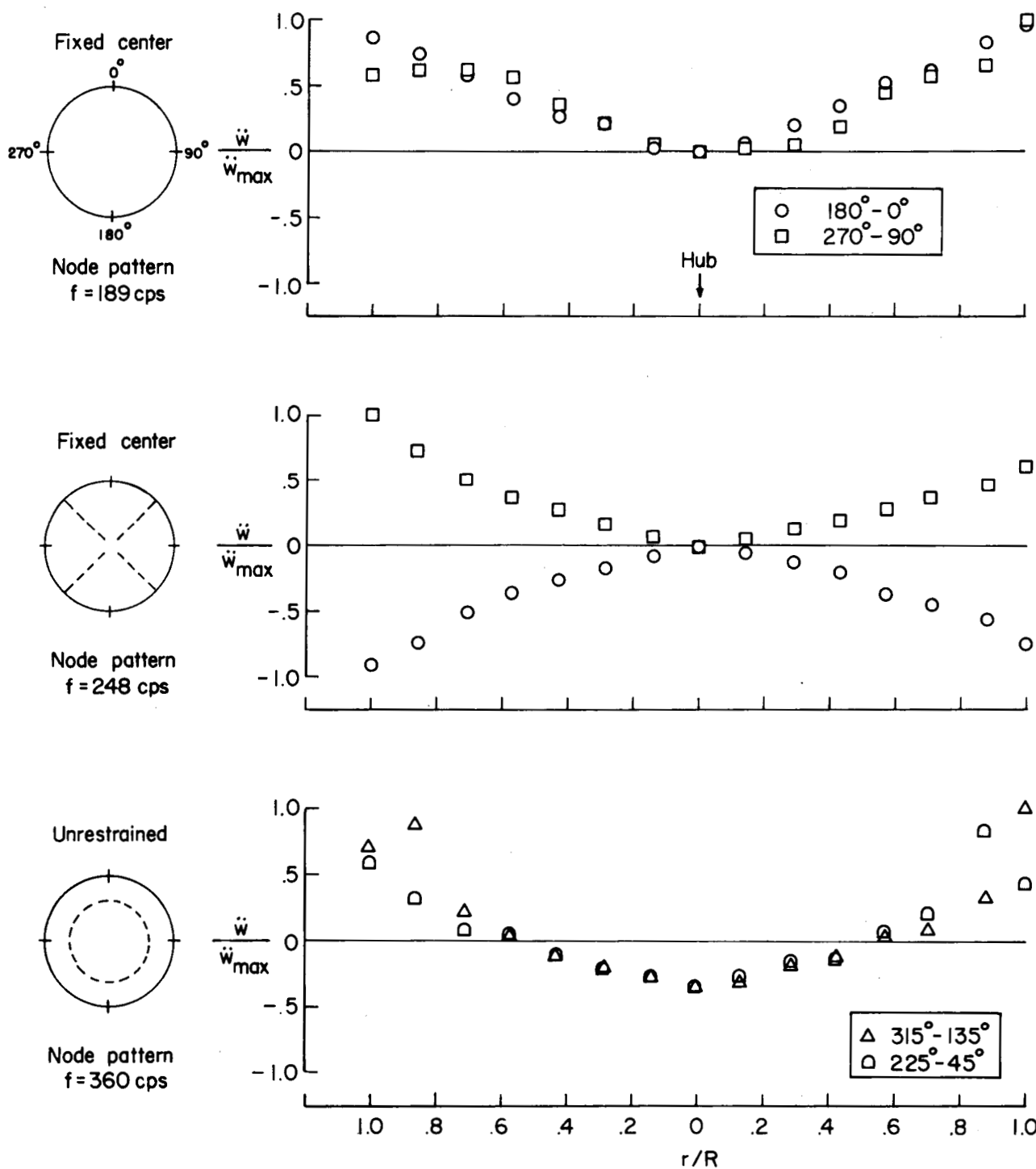


Figure 10.- Honeycomb-core measured mode shapes. H-3 model.

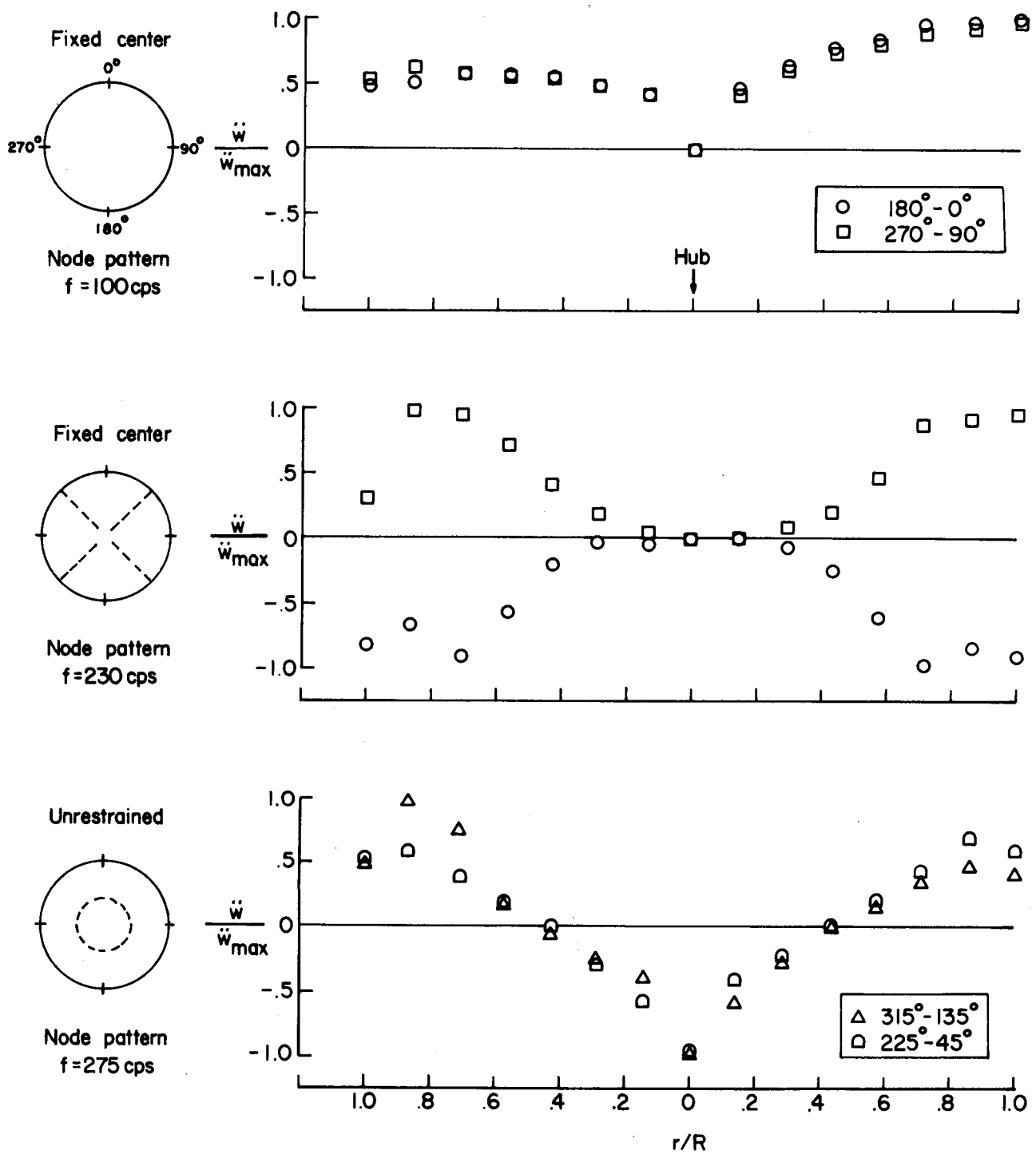


Figure 11.- Styrofoam-core measured mode shapes. F-3 model.

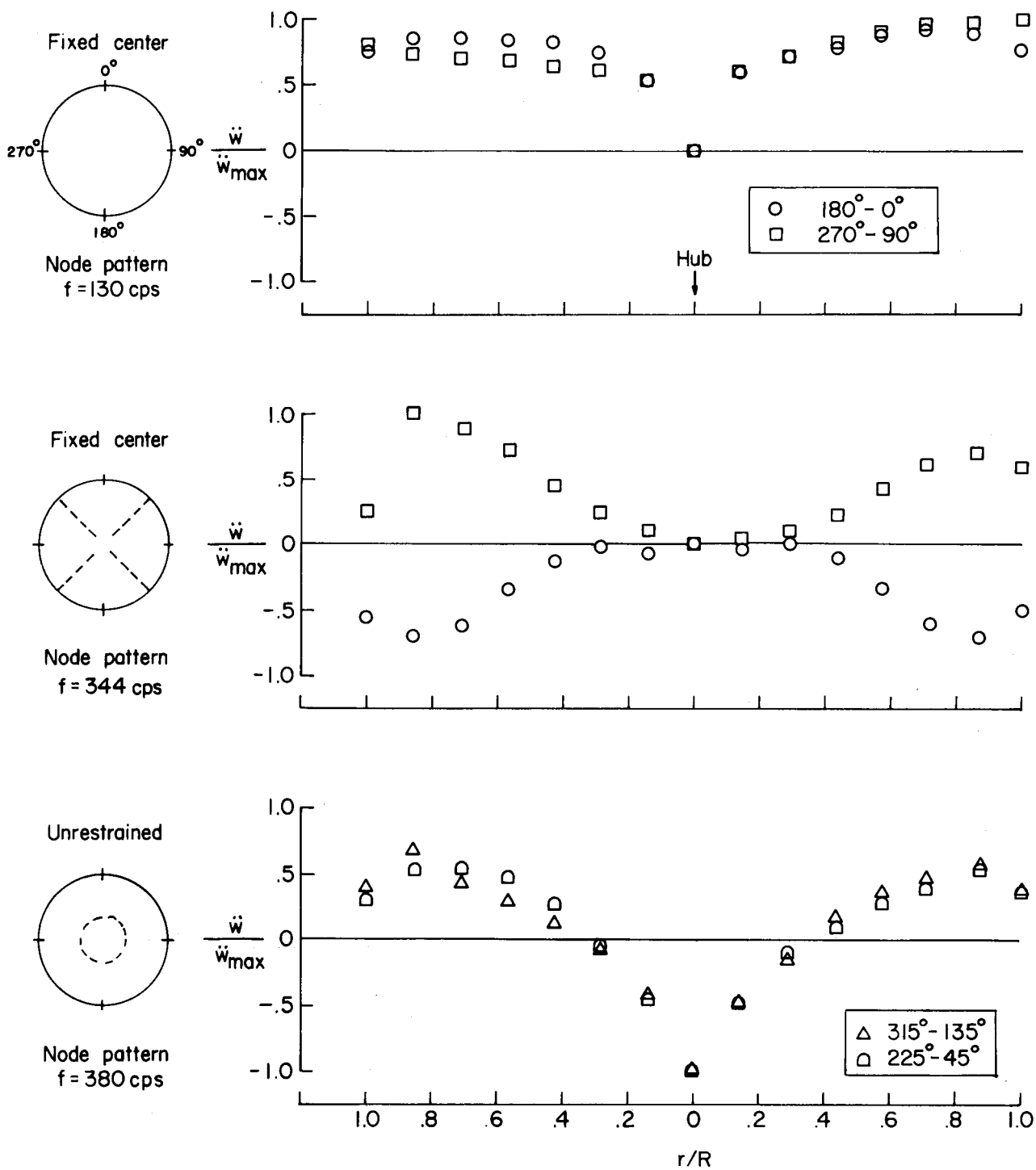


Figure 12.- Styrofoam-core measured mode shapes. F-6 model.

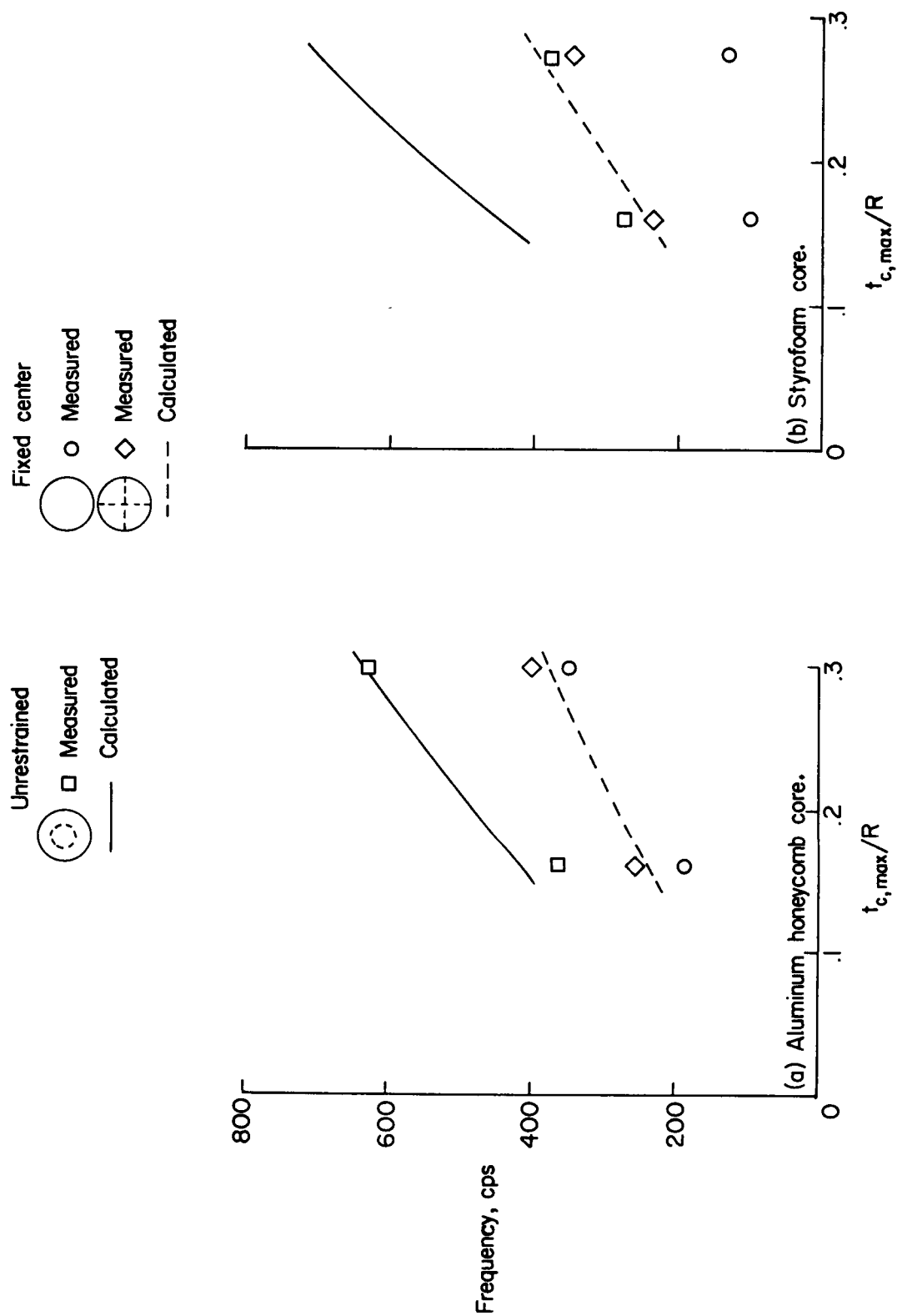
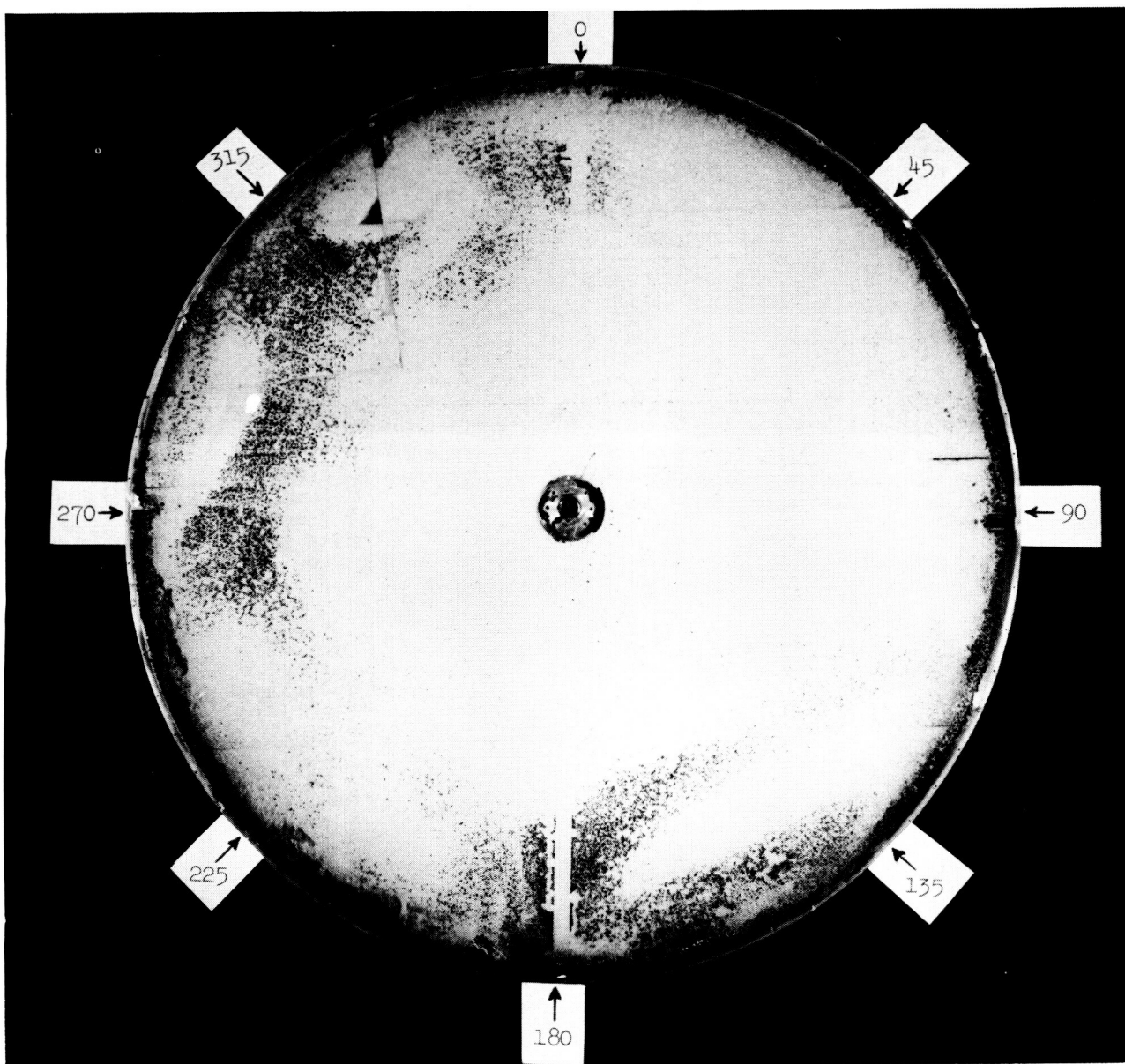


Figure 14.- Comparison of calculated and measured natural frequencies.



L-63-1016

Figure 13.- Styrofoam core of F-3 model after removal of face plate. (Shaded areas away from rim indicate regions where bonding was not achieved.)